



Facile morphology-controlled synthesis of nanostructured MnMoO₄ nanorods as an advance electrode material for supercapacitor application

G. Harichandran¹ · S. Radha¹ · P. Divya¹ · J. Yesuraj²

Received: 29 September 2019 / Accepted: 2 December 2019 / Published online: 9 December 2019
© Springer Science+Business Media, LLC, part of Springer Nature 2019

Abstract

A facile microwave-assisted method has been successfully established for the preparation of manganese molybdate (MnMoO₄) materials. The surface morphologies of the MnMoO₄ specimens were altered by varying the duration of microwave irradiation, and various morphologies such as rounded rectangular shaped nanosheets and ultra-small nanorod structures have been attained. The proposed use of MnMoO₄ as an active electrode material for supercapacitor application was evaluated by cyclic voltammetric and chronopotentiometric measurements. It is interesting to note that the observed specific capacitance of the MnMoO₄ electrode depends on its surface morphology. A unique one-dimensional MnMoO₄ demonstrated excellent electrochemical properties, which provide 836 Fg⁻¹ of specific capacitance at a scan rate of 5 mVs⁻¹ with an excellent cycling stability (84% of the initial specific capacitance retained after 3000 cycles). These outstanding electrochemical features of MnMoO₄ materials may be associated with their inherent properties such as small size, distinctive nanorod architecture and intriguing physicochemical properties. These results will render the MnMoO₄ materials as new and attractive active material for promising application in supercapacitors.

1 Introduction

Supercapacitor, a new generation energy storage device, demonstrated the applications of instant power supply with high-energy density and long-term cycling stability leading to application in hybrid electric vehicles, memory back up, military, medical, aerial lift, public transport, etc., [1–3]. The supercapacitor, an eco-friendly energy device, has abated the boundaries of the other two conventional energy sources, namely rechargeable battery and capacitor, in terms of both high-energy and power densities [4]. Supercapacitors can be categorised into two types—electric double-layer capacitor and pseudocapacitor. Electron transfer (faradaic) reactions occur in pseudocapacitor which stores enormous amount of electrical energy. On the other hand, electrical double layer is designed by the electrostatic interaction between the

oppositely charged ions at the active electrode material/electrolyte interface in electric double-layer capacitor (EDLC). Activated carbon, aerogel, carbon nanotubes and graphene nanosheets have been utilized as EDLC electrode materials. Transition metal oxide/hydroxide nanostructures and conducting polymers have been used for pseudocapacitance applications [5–7]. Materials such as Co(OH)₂ [8], Ni(OH)₂ [9], SnO₂ [10], MnO₂ [11], MoO₃ [12] and Co₃O₄ [13] have also been extensively demonstrated as pseudocapacitive electrode materials. However, there are some limitations such as high cost and toxicity of RuO₂, and poor electrical conductivity of MnO₂ which restricts their application in supercapacitor devices [14, 15].

Presently, binary metal oxides such as CoMoO₄ [16], NiMoO₄ [17], MnMoO₄ [18], and their carbon composites have shown much interest due to their low-cost, feasible oxidation states, better electrical conductivity and good thermal and chemical stability to accomplish superior electrochemical performance. Additionally, the metal ions of the binary metal oxides offer rich redox reactions. Among these binary metal oxides, MnMoO₄ has been of much interest owing to its low-cost, eco-friendliness, high electrical conductivity, large working voltage window and excellent stability. For example, Liu et al. demonstrated rod-like

✉ G. Harichandran
umghari@gmail.com

¹ Department of Polymer Science, University of Madras, Guindy Campus, Chennai 600 025, India

² Department of Energy, University of Madras, Guindy Campus, Chennai 600 025, India

manganese molybdate, which exhibited 109 Cg^{-1} at a current density of 1 Ag^{-1} and provide good cyclic stability [19]. Zhang et al. synthesized $\text{MnMoO}_4 \cdot n\text{H}_2\text{O}$ nanosheets, which delivered 1271 Fg^{-1} at a scan rate of 5 mVs^{-1} and retained 84.5% of its initial capacitance after 2000 cycles [20]. The $\text{MnMoO}_4 \cdot 4\text{H}_2\text{O}$ nanoplates provided a specific capacitance of 2300 Fg^{-1} at a current density of 4 mA cm^{-2} and offered higher cyclic stability [21]. The $\alpha\text{-MnMoO}_4$ fan-like nanostructures exhibited a specific capacitance of 562 F g^{-1} at a current density of 1 A g^{-1} and good cycling stability with 99.8% specific capacitance retained after 1000 cycles [18]. Veerasubramani et al. prepared MnMoO_4 nanorods, which gave a specific capacitance of 168.32 F g^{-1} at a current density of 0.5 mA cm^{-2} and long-term cycling stability [22]. However, the synthesis of MnMoO_4 by a simple, eco-friendly and reliable method remains a massive challenge.

Various methods of synthesis such as sol–gel, hydrothermal and precipitation have been utilized to create the principle-oriented nanostructures [23]. Among them, microwave-assisted synthesis has been widely used to prepare oxides, hydroxides and sulphide-based metal oxides. Fascinatingly, this method is clean and simple, and there are no complications due to thermal gradient effect. In addition, this approach has advantages such as faster reaction, simple medium, lesser time to achieve the appropriate temperature for reaction process, formation of principle-oriented nanostructures when compared to hydrothermal method [24, 25]. Bensebaa et al. prepared polymer coated platinum–ruthenium nanoparticles using microwave-assisted method [26]. Hasanpoor et al. synthesized zinc oxide nanomaterials via microwave-assisted method. There are numerous other studies on the utility of microwave method for preparing nanomaterials [27].

In the present effort, MnMoO_4 nanorods have been synthesized using microwave method without any surfactant. The growing process of MnMoO_4 nanorod structures has been altered by controlling the reaction time. The freshly prepared MnMoO_4 nanorods provide a specific capacitance of 836 Fg^{-1} at a scan rate of 5 mVs^{-1} , with 84% retention after 3000 cycles.

2 Experimental methods

2.1 Materials

Analar grade sodium molybdate dihydrate ($\text{Na}_2\text{MoO}_4 \cdot 2\text{H}_2\text{O}$), manganese acetate tetrahydrate ($\text{Mn}(\text{CH}_3\text{COO})_2 \cdot 4\text{H}_2\text{O}$), potassium hydroxide and sodium hydroxide were purchased from Sisco Research Laboratories Pvt. Ltd. (India). Carbon black, polyvinylidene difluoride (PVDF) and *N*-methyl-2-pyrrolidone (NMP) were purchased from Loba Chemie Pvt. Ltd. (India). Nickel foil (0.025 mm thickness), 99.5%

(metal basis), was acquired from Alfa Aesar (India). All reagents were used without any further purification. The synthesis was carried out in a domestic microwave oven, Kenstar 3D power. Double distilled water was used for all the preparation and measurements.

2.2 Synthesis of MnMoO_4 materials

The one-dimensional MnMoO_4 nanorods were synthesized via microwave-assisted method using manganese acetate and sodium molybdate as the starting precursors. In this method, about 500 mmol of manganese acetate was dissolved in 50 ml of isopropanol–water mixture (1:1 V/V). Then, 500 mmol of sodium molybdate was also dissolved in 50 ml of isopropanol–water mixture separately. Sodium molybdate solution was added dropwise into manganese acetate solution with continuous stirring. The pH of the mixture was adjusted to 10 by the addition of NaOH. The mixture was then heated in a microwave oven for 20 min. The resultant slurry was repeatedly washed with distilled water–alcohol mixture, filtered and dried at $60 \text{ }^\circ\text{C}$ in a vacuum oven for 12 h. The dried material was calcined at $300 \text{ }^\circ\text{C}$ for 3 h. The synthesis was also carried out at different durations of microwave treatment—20, 40, 60 and 80 min. The specimens were designated as $\text{MnMoO}_4\text{-20}$, $\text{MnMoO}_4\text{-40}$, $\text{MnMoO}_4\text{-60}$ and $\text{MnMoO}_4\text{-80}$ corresponding to 20, 40, 60 and 80 min of microwave irradiation time, respectively.

2.3 Materials characterisation

The powder X-ray diffraction (XRD) patterns were analysed from $2\theta = 10^\circ$ to 80° using PANalytical X-pert PRO diffractometer with Cu-K α radiation ($\lambda = 0.154060 \text{ nm}$, 40 kV and 30 mA) at a scan rate of $0.07^\circ \text{ s}^{-1}$. Fourier transform infrared (FTIR) spectra were recorded in the range 4000 to 400 cm^{-1} using a ‘Perkin-Elmer RX1’ spectrophotometer with 4 cm^{-1} resolution for 20 scans. Raman spectra were measured in the range 2000 to 250 cm^{-1} with a ‘Confocal Raman I-11 Model’ spectrophotometer (Nanophoton Corp., Japan) using a 532 nm source from an argon ion laser. The morphological features and SAED patterns were examined in field-emission scanning electron microscope (FE-SEM, Hitachi SU6600) and high-resolution transmission electron microscope (HRTEM, Techni G2S-TWIN, FEI), respectively.

2.4 Electrode preparation

The working electrodes of all the freshly prepared MnMoO_4 samples were fabricated by the following procedure: The active material, carbon black and poly(vinylidene fluoride) (PVDF) were ground at a mass ratio of 80:10:10. Required amount of *N*-methylpyrrolidone (NMP) solvent was added to the mixture and ground satisfactorily to get a paste. Then, the

paste was uniformly coated on the nickel foil substrate and dried in a vacuum oven at 60 °C for 24 h. The active mass of the materials was ~2 mg for all the MnMoO₄ electrodes. For the three-electrode configuration, the active material coated on nickel foil, Pt wire and saturated calomel electrode served as working, counter and reference electrodes, respectively. The fabricated electrodes were evaluated by cyclic voltammetry (CV) and chronopotentiometric (CP) techniques using Biologic (model SP-150) electrochemical workstation in an alkali 1 M KOH electrolyte. CV analysis were done at various scan rates from 5 to 100 mVs⁻¹, in the potential window between 0 and 0.5 V, and CP tests were performed at different current densities such as 1, 2, 3, 10 and 15 Ag⁻¹, between 0 and 0.45 V potential window. The cycling stability measurement was taken at a scan rate of 100 mVs⁻¹ for continuous 3000 cycles.

3 Results and discussion

The crystalline nature, phase and purity of freshly prepared MnMoO₄ specimens were evaluated using X-ray diffraction analysis. Figure 1a, b, c and d shows the XRD patterns of MnMoO₄-20, MnMoO₄-40, MnMoO₄-60 and MnMoO₄-80 specimens, respectively. All the XRD patterns displayed well-defined diffraction peaks matching with the standard data (JCPDS card no. 01-072-0285) and indexed to the monoclinic phase (C2/m), confirming the presence of

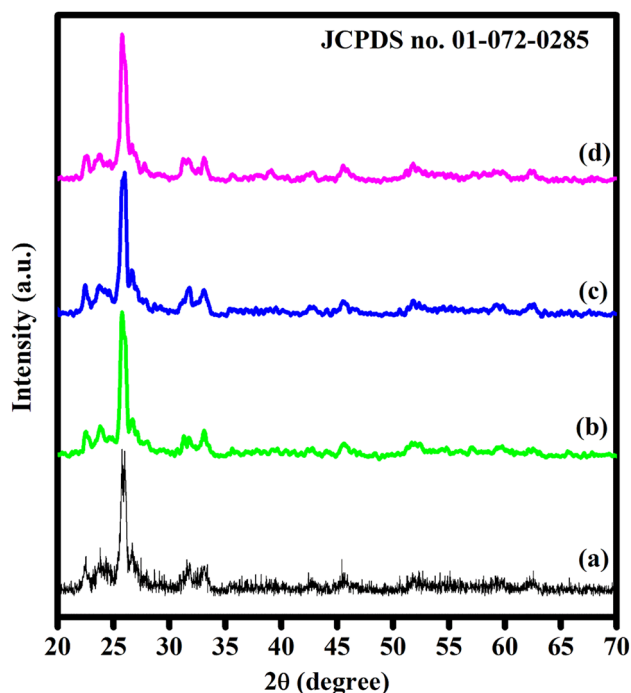


Fig. 1 XRD patterns of the prepared MnMoO₄ materials a MnMoO₄-20; b MnMoO₄-40; c MnMoO₄-60; d MnMoO₄-80

pure crystalline MnMoO₄ samples [28]. All the observed major diffraction peaks at 2θ values of 22.7°, 24.7°, 25.7°, 25.9°, 26.6°, 27°, 27.7°, 31.2°, 32.1°, 33°, 35.7°, 37.7°, 39°, 40.4°, 45.6°, 45.9°, 51.2°, 52.3°, 52.9°, 57° and 59.3° were indexed to the lattice planes (021), (201), (220), (002), (-112), (-202), (-311), (112), (022), (-222), (400), (040), (-113), (222), (241), (421), (-204), (-531), (440), (024) and (-424), respectively. The nonappearance of diffraction peaks due to Mn- or Mo-based oxides confirms the formation high purity MnMoO₄ materials. In addition, the broad diffraction peaks of all MnMoO₄ specimens also indicate their nanocrystalline nature. Irrespective of the duration of microwave treatment, all the MnMoO₄ materials exhibit the same diffraction pattern with minor variations in peak intensities.

The bonding nature and internal properties of the freshly prepared MnMoO₄ specimens were examined using Raman and FTIR spectroscopic analysis. Figure 2 shows the Raman spectra of MnMoO₄ specimens and the bands that appear at 923, 870, 814, 350, 326 and 273 cm⁻¹ are the representative bands of MnMoO₄. The bands appearing in higher wave number region (943 to 810 cm⁻¹) are due to the stretching vibrations of tetrahedral MoO₄⁻ ions and the peaks in the region of 400 to 250 cm⁻¹ are attributed to the bending vibrations of tetrahedral MoO₄⁻ ions [28–30]. These results are further confirmed by FTIR analysis. The FTIR spectra of MnMoO₄ specimens shown in Fig. 3 exhibit six strong bands at 927, 900, 860, 790, 745 and 703 cm⁻¹ which are the corresponding peaks of MnMoO₄. The band at 927 cm⁻¹ is attributed to the stretching vibration of the Mo=O group.

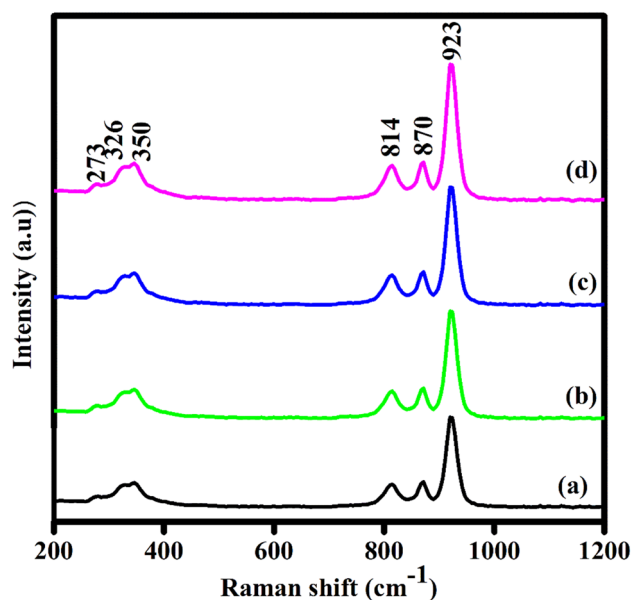


Fig. 2 Raman spectra of the prepared MnMoO₄ materials a MnMoO₄-20; b MnMoO₄-40; c MnMoO₄-60; d MnMoO₄-80

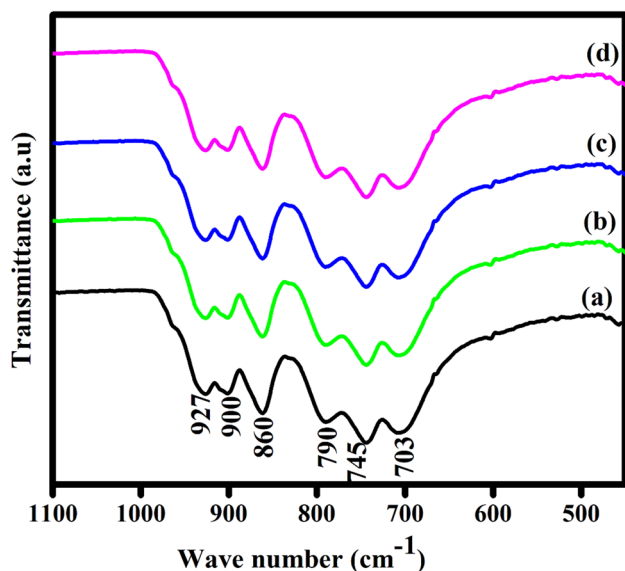


Fig. 3 FTIR spectra of the prepared MnMoO_4 materials **a** MnMoO_4 -20; **b** MnMoO_4 -40; **c** MnMoO_4 -60; **d** MnMoO_4 -80

The bands at 900 and 860 cm^{-1} are due to the Mo–O–Mo bending vibrations. The bands at 790 and 745 cm^{-1} are the characteristic bands of the Mo–O stretching vibration in the tetrahedral MoO_4 groups [29, 31, 32]. The basic characterisation results (XRD, Raman and FTIR) confirm the formation of MnMoO_4 specimens through microwave-assisted synthesis method.

The morphology of MnMoO_4 specimens was studied by SEM. Figure 4a, b shows the low- and high-magnification SEM images of MnMoO_4 -20 specimen, which reveal a few elongated rectangular nanosheets of ~ 95 nm breadth and 400 nm length with curved edges. In addition, irregular

shaped nanosheets are also observed. Increasing the irradiation time to 40 min (MnMoO_4 -40) leads to formation of nanorods of ~ 110 nm breadth and 500 nm length (Fig. 4c, d). The nanorods are not uniform and are accompanied by several ultra-small nanoparticles. Figure 4e, f shows the lower and higher magnification images of MnMoO_4 -60 specimen. Here, we observe an increase in nanorod content (breadth and length are ~ 90 and 300 nm, respectively) and a decrease in the number of ultra-small particles. MnMoO_4 -80 specimen is made of uniform nanorods of size ~ 30 nm and length 75 nm and is devoid of the ultra-small particles. From these results, it is clear that the microwave irradiation time and microwave irradiation were controlling the morphology of the MnMoO_4 nanomaterials.

The MnMoO_4 -80 specimen was studied by HRTEM analysis. The bright field images (Fig. 5a, b) show short nanorods in consistence with the SEM results. The high-resolution image (Fig. 5c) shows lattice fringes with an inter-planar spacing of ~ 3.4 Å due to the (220) crystallographic plane. The selected area electron diffraction (SAED) pattern of the MnMoO_4 -80 specimen (Fig. 5d) shows spots corresponding to d-spacings of ~ 3.4 and 2.2 Å due to (220) and (222) crystallographic planes, respectively.

To examine the electrochemical features of MnMoO_4 materials, the CV analysis was performed with a three-electrode configuration in aqueous 1 M KOH electrolyte solution at the scan rates of 5, 10, 20, 40, 50, 60, 70, 80, 90 and 100 mV s^{-1} in the voltage range from 0 to 0.5 V. The CV curves (Fig. 6) displayed the redox peaks due to the $\text{Mn}^{2+}/\text{Mn}^{3+}$ redox couple confirming the pseudocapacitive nature of the materials. At a lower scan rate of 5 mVs^{-1} , the anodic peak observed at around 0.3 V indicates the oxidation of Mn^{2+} to Mn^{3+} , while the cathodic peak at around 0.2 V is owing to the reduction of Mn^{3+} to Mn^{2+} [19, 28]. During the CV measurements, the

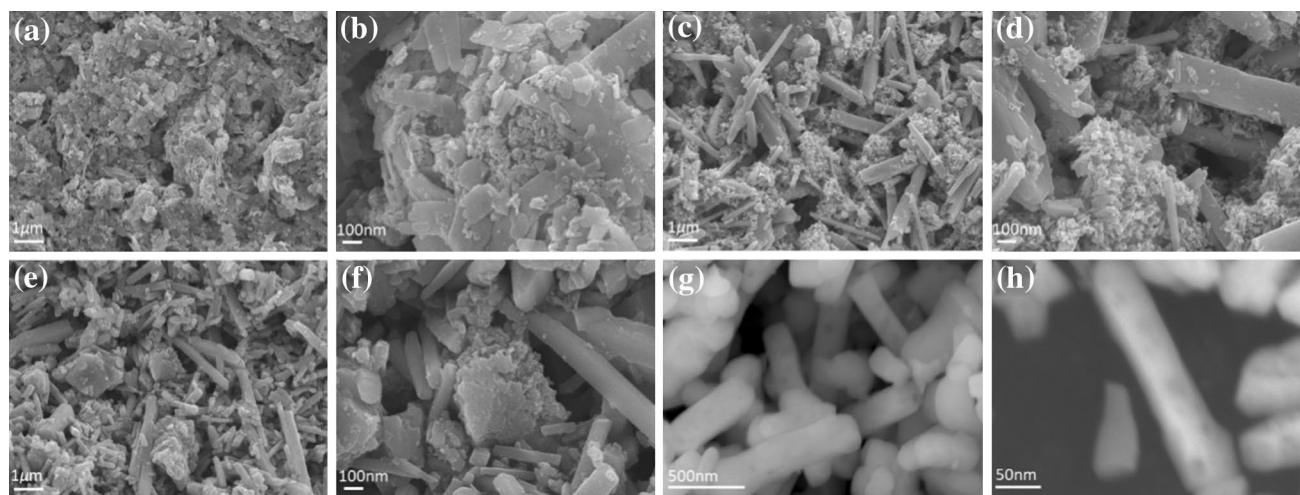
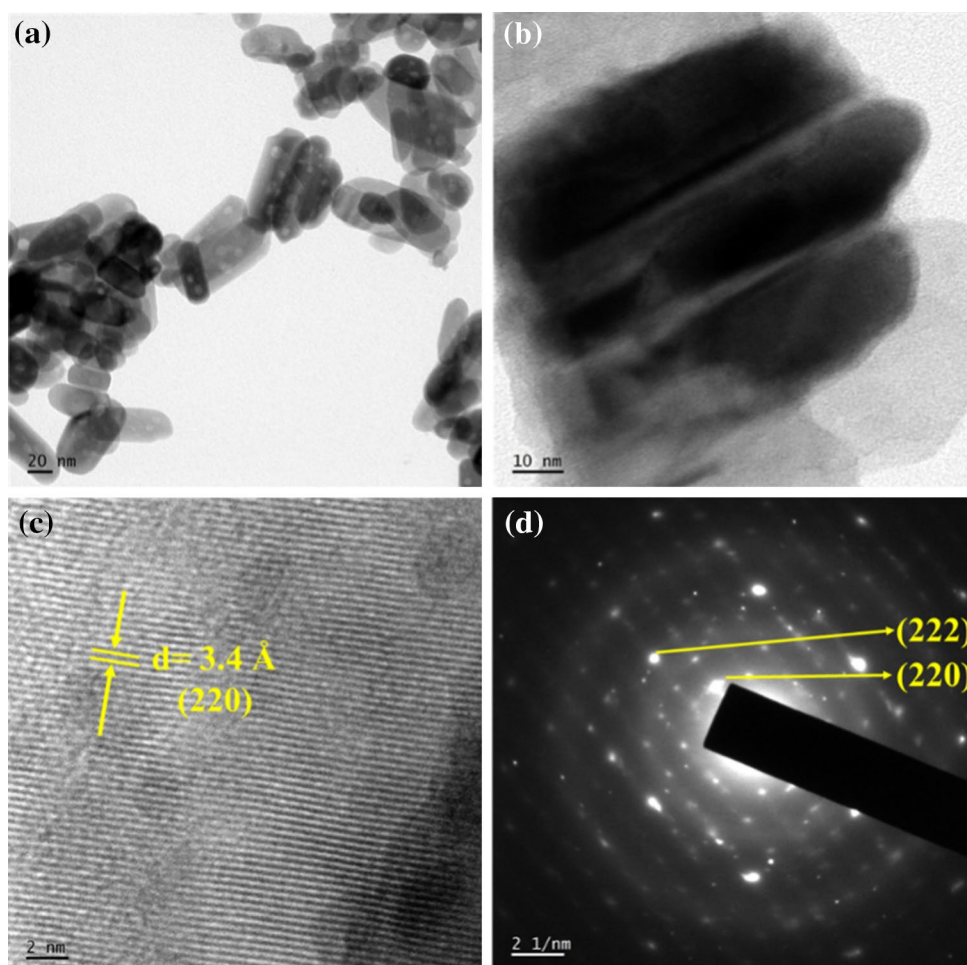


Fig. 4 Lower and higher magnification FE-SEM images of the prepared MnMoO_4 materials **a** and **b** MnMoO_4 -20; **c** and **d** MnMoO_4 -40; **e** and **f** MnMoO_4 -60; **g** and **h** MnMoO_4 -80

Fig. 5 Lower and higher magnification TEM bright field images (a) and (b); HRTEM (c); and SAED pattern (d) of MnMoO₄-80



molybdate (Mo) ions do not participate in any electrochemical redox reactions, but they endorse the electrical conductivity of MnMoO₄ materials [33]. It is interesting to note that the shape profile of the CV curves does not change at high scan rates (100 mVs⁻¹) indicating superior capacitive behaviour. When increasing the scan rate from 5 to 100 mVs⁻¹, the anodic peak shifts to more positive potential and the cathodic peak shifts to more negative potential. This suggests that the ionic and electronic movements are fast, and a rapid redox reaction arises at the electrode/electrolyte interface at higher scan rates, [34, 35]. Figure 6e shows the CV curves of MnMoO₄-20 and MnMoO₄-80 electrodes at a scan rate 5 mVs⁻¹. The area under the curve of the MnMoO₄-80 electrode is higher when compared to other electrode materials such as MnMoO₄-20 due to better electron conduction and the higher extent of redox pseudocapacitance [36]. The specific capacitance values were calculated from the CV curves using Eq. 1:

$$C_{\text{sp}} = \frac{\int idv}{2 \cdot S \cdot \Delta V \cdot m} \quad (1)$$

where $\int idv$ denotes the integral area of CV curve, m mass of the active material (mg), ΔV potential window (V) and S is the scan rate (mV s⁻¹). The specific capacitance values of the MnMoO₄-20, MnMoO₄-40, MnMoO₄-60 and MnMoO₄-80 specimens are 197, 351, 478 and 836 Fg⁻¹, respectively, at a scan rate 5 mVs⁻¹. The MnMoO₄-80 electrode produced ~4 times enhancement in the capacitance compared to the MnMoO₄-20 sample owing to the existence of uniform one-dimensional nanorods. Significantly, the specific capacitance of MnMoO₄-80 is greater than those of MnMoO₄ (200 Fg⁻¹) [37], α -MnMoO₄ nanorods (551 Fg⁻¹) [38], α -MnMoO₄/graphene hybrid composite (364 Fg⁻¹) [29] and MnMoO₄ nanorods (168.32 Fg⁻¹) [22] reported earlier in the literature. The resultant superior capacitance may be owing to the following: (i) One-dimensional morphology of the nanorods induces the separation between the two nanorods and makes most surface area of nanorods proficiently accessible by electrolyte ions. (ii) Nanorods offer high surface area which act as a H⁺ ion transfer source and provide good interaction, diffusion and distribution of H⁺ ions for faster electrode kinetics and high reversible redox progressions for charge storage. (iii) Both

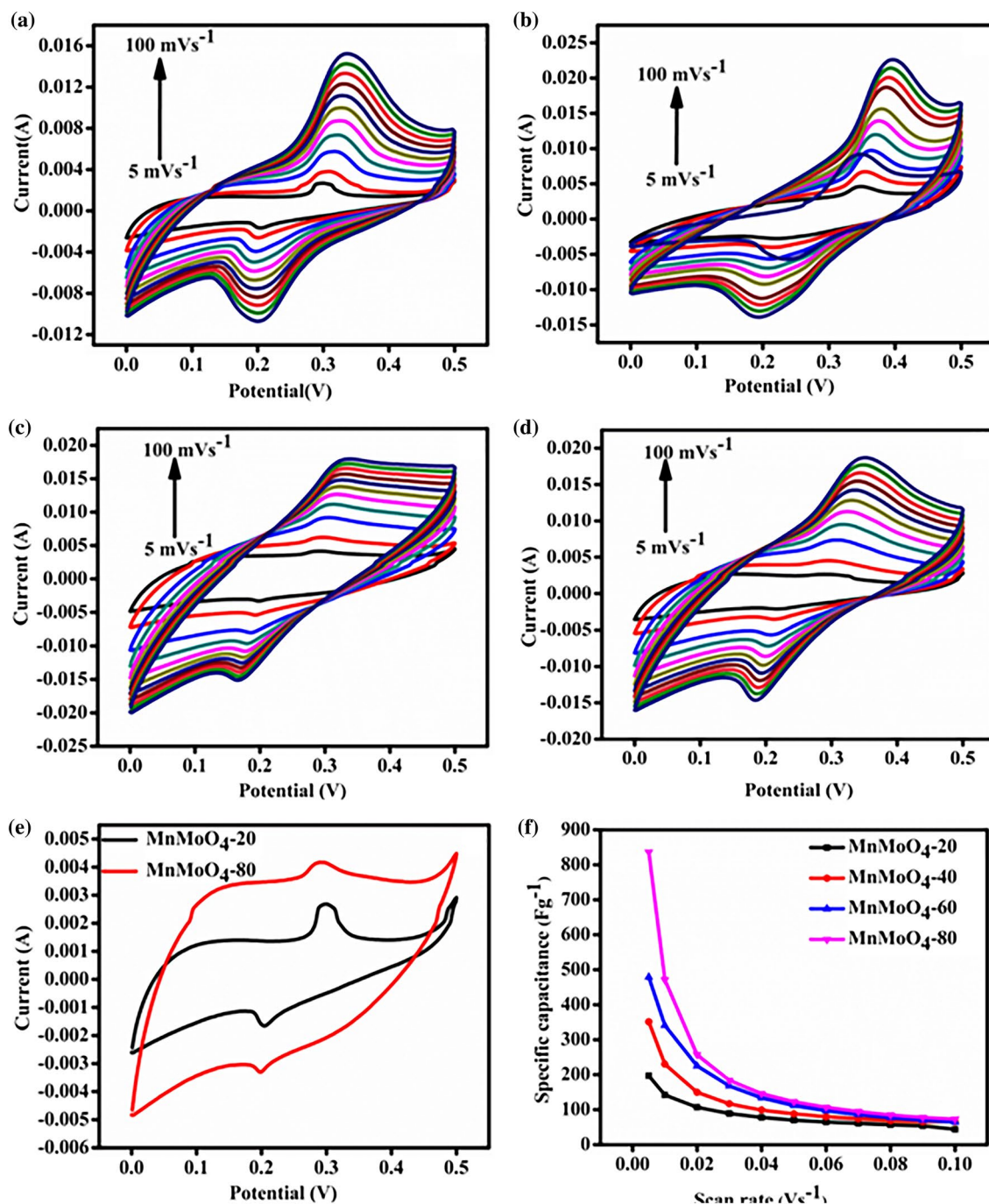


Fig. 6 Cyclic voltammetric curves at six different scan rates for **a** MnMoO₄-20, **b** MnMoO₄-40, **c** MnMoO₄-60, **d** MnMoO₄-80; **e** CV curves of MnMoO₄-20 and MnMoO₄-80 at a scan rate of 5 mV s⁻¹; **f** Scan rate vs specific capacitance for MnMoO₄-80

Mn and Mo species are good supercapacitor species, whose combination provides multifunctional effects. The specific capacitance vs scan rate graph for MnMoO₄-80 is displayed in Fig. 6f. Due to time limitation phenomena, the specific capacitance decreases with increasing scan rate. At higher scan rates, the distribution of electrolyte ions is restricted by the rate at which the potential varies. However, at lower

scan rates, more of the active sites of the electrode materials are well used to help the propagation of the electrolyte ions. This is helpful in proficient charge storage and leads to an elevated specific capacitance. [39, 40].

To further examine the electrochemical features of MnMoO₄-80 electrode, chronopotentiometric (CP) measurements were taken at room temperature. The CP curves

(Fig. 7a) exhibit a plateau, signifying a faradaic redox reaction at the electrode/electrolyte interface. The voltage–time curve demonstrates symmetric charge–discharge characteristics at various current densities, signifying outstanding pseudocapacitive features and admirable reversible redox behaviour [41]. The CP curve exhibits two characteristics: (i) The rapid discharge profile occurred between 0.45 and 0.25 V (approximately) due to the resistance of the prepared MnMoO_4 material. (ii) The presence of curved region (0.25 to 0 V) indicates the supercapacitive behaviour. Specific capacitances of MnMoO_4 -80 electrode specimen can be estimated from charge–discharge curves according to the equation:

$$C_{\text{sp}} = \frac{I\Delta t}{m\Delta V} \quad (2)$$

where ΔV denotes potential window (V), m mass of the active material (mg), I (A) discharge current density and Δt (s) is the discharge time. The discharge specific capacitance values are calculated to be 733, 413, 280, 111 and 100 Fg^{-1} at the current densities of 1, 2, 3, 10 and 15 Ag^{-1} , respectively. Figure 7b shows the specific capacitance vs current density graph which resembles the specific capacitance vs scan rate graph (Fig. 6f).

Good cycling stability is also a significant feature of the electrode materials for their potential application in supercapacitors. The cycling stability of MnMoO_4 -80 electrode was assessed by means of CV measurements at a scan rate 100 mVs^{-1} for 3000 cycles (Fig. 8). It is interesting to note that the specific capacitance increases at initial cycles, which indicates the activating progression of the electrode material [42]. After that the specific capacitance slowly decreases and attains 84% of its initial specific capacitance value after 3000 CV cycles. The 1st, 1000th, 2000th and 4000th CV curves of

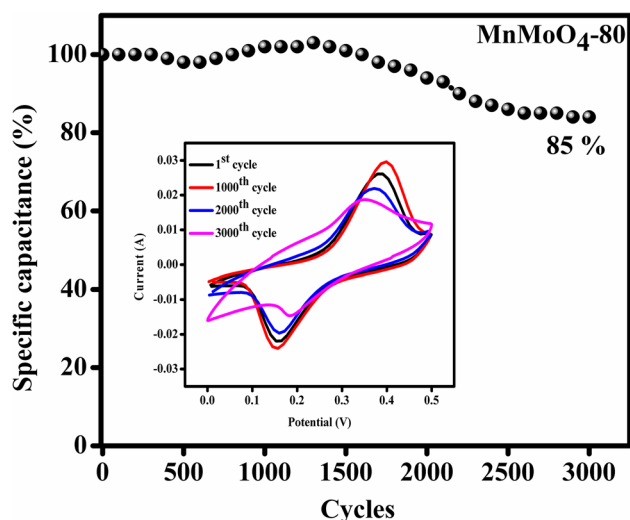


Fig. 8 Cycling stability of MnMoO_4 -80 specimen at a scan rate of 100 mVs^{-1} for 3000 cycles; Inset: Cyclic voltammograms at 1, 1000, 2000, 3000th cycles

cyclic stability studies are shown in the inset of Fig. 8. The enhanced cycling stability demonstrated by MnMoO_4 -80 electrode is due to its high structural stability. These findings indicate that MnMoO_4 -80 could be considered a competent supercapacitor electrode material.

4 Conclusion

Manganese molybdate with varying surface morphology was synthesized by means of a microwave-assisted method. The present effort affords a new feature to change the growth conditions leading to various morphologies such as nanosheets

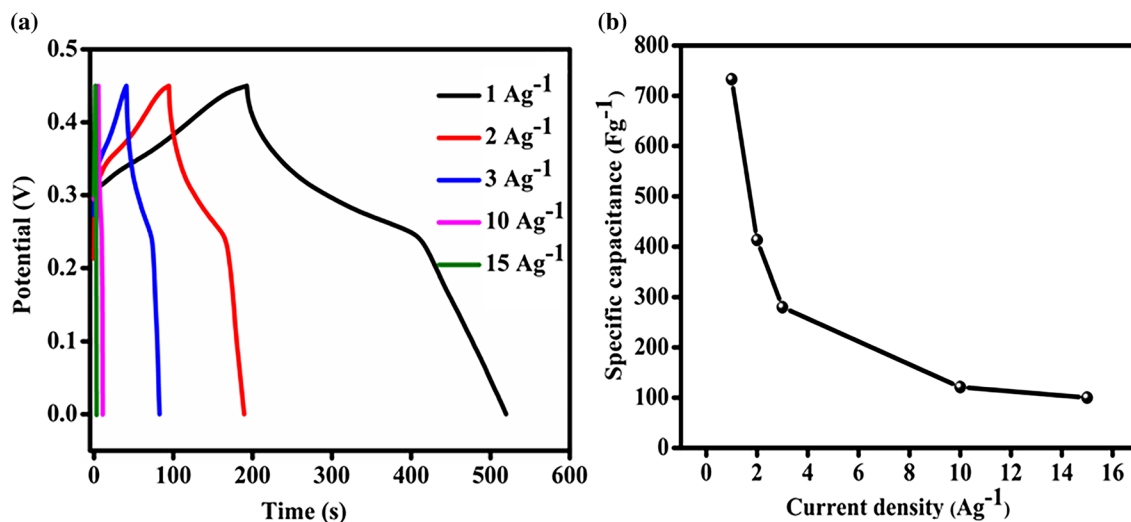


Fig. 7 a Chronopotentiometric curves at different current densities and b Current density vs specific capacitance for MnMoO_4 -80

and nanorods. The supercapacitive properties of these specimens were evaluated using CV and CP techniques. The CV analysis of MnMoO₄ specimens confirms their pseudocapacitive nature. The MnMoO₄ nanorod sample (MnMoO₄-80) delivered a superior specific capacitance of 836 Fg⁻¹ at a scan rate 5 mVs⁻¹ with good rate capability. Additionally, MnMoO₄-80 exhibited excellent cyclic stability of 84% retention over 3000 cycles of continuous CV analysis at a scan rate 100 mVs⁻¹. Owing to its outstanding electrochemical performances such as superior specific capacitance, high rate capability and excellent cyclic stability, the prepared MnMoO₄ nanorod sample (MnMoO₄-80) could be a favourable candidate for next-generation supercapacitors.

Acknowledgements One of the authors GH acknowledges DST (SB/EMEQ-101/2013) for funding the project. Authors thank Dr Michel Rajamathi for XRD measurements and for fruitful discussions.

References

- J.S. Lee, D.H. Shin, W. Kim, J. Jang, *J. Mater. Chem. A* **4**, 6603 (2016)
- X. Pan, X. Chen, Y. Li, Z. Yu, *Electrochim. Acta* **182**, 1101 (2015)
- W. Chen, R.B. Rakhi, L. Hu, X. Xie, Y. Cui, H.N. Alshareef, *Nano Lett.* **11**, 5165 (2011)
- H.W. Chang, Y.R. Lu, J.L. Chen, C.L. Chen, J.F. Lee, J.M. Chen, Y.C. Tsai, P.H. Yeh, W.C. Chou, C.L. Dong, *Phys. Chem. Chem. Phys.* **18**, 18705 (2016)
- N. Wang, Q. Liu, D. Kang, J. Gu, W. Zhang, D. Zhang, *A.C.S. Appl. Mater. Interfaces* **8**, 16035 (2016)
- C. Zhang, Q. Chen, H. Zhan, *A.C.S. Appl. Mater. Interfaces* **8**, 22977 (2016)
- S. Wang, S. Sun, S. Li, F. Gong, Y. Li, Q. Wu, P. Song, S. Fang, P. Wang, *Dalton Trans.* **45**, 7469 (2016)
- J. Li, P. Yang, X. Cheng, X. Zhang, K. Ding, *CrystEngComm* **19**, 5780 (2017)
- X. Guo, M. Xie, Z. Xu, Y. Zhang, M. Lin, W. Ding, K. Xiang, Z. Tian, S. Duan, *Nano Res.* **11**, 216 (2017)
- Y. Liu, Y. Jiao, Z. Zhang, F. Qu, A. Umar, X. Wu, *A.C.S. Appl. Mater. Interfaces* **6**, 2174 (2014)
- M. Huang, F. Li, F. Dong, Y.X. Zhang, L.L. Zhang, *J. Mater. Chem. A* **3**, 21380 (2015)
- B. Mendoza-Sánchez, T. Brousse, C. Ramirez-Castro, V. Nicolosi, P.S. Grant, *Electrochim. Acta* **91**, 253 (2013)
- J. Tu, C. Gu, X. Zhao, X. Wang, Y. Zhang, X. Xia, Y. Mai, *RSC Adv.* **2**, 1835 (2012)
- Q. Guan, J. Cheng, B. Wang, W. Ni, G. Gu, X. Li, L. Huang, G. Yang, F. Nie, *A.C.S. Appl. Mater. Interfaces* **6**, 7626 (2014)
- V. Veeramani, R. Madhu, S.M. Chen, M. Sivakumar, *A.C.S. Sustainable, Chem. Eng.* **4**, 5013 (2016)
- R. Ramkumar, M. Minakshi, *Dalton Trans.* **44**, 6158 (2015)
- K. Xiao, L. Xia, G. Liu, S. Wang, L.X. Ding, H. Wang, *J. Mater. Chem. A* **3**, 6128 (2015)
- L. Wang, L. Yue, X. Zang, H. Zhu, X. Hao, Z. Leng, X. Liu, S. Chen, *CrystEngComm* **18**, 9286 (2016)
- H. Cao, N. Wu, Y. Liu, S. Wang, W. Du, J. Liu, *Electrochim. Acta* **225**, 605 (2017)
- X. Mu, Y. Zhang, H. Wang, B. Huang, P. Sun, *Electrochim. Acta* **211**, 217 (2016)
- Y. Cao, W. Li, K. Xu, Y. Zhang, T. Ji, R. Zou, J. Yang, Z. Qin, J. Hu, *J. Mater. Chem. A* **2**, 20723 (2014)
- G.K. Veerasubramani, K. Krishnamoorthy, R. Sivaprakasam, S.J. Kim, *Mater. Chem. Phys.* **147**, 836 (2014)
- S.R. Ede, A. Ramadoss, S. Anantharaj, U. Nithiyantham, S. Kundu, *Phys. Chem. Chem. Phys.* **16**, 21846 (2014)
- W. Yu, W. Tu, H. Liu, *Langmuir* **15**, 6 (2002)
- X.C. Xu, Y. Bao, C.S. Song, W.S. Yang, J. Liu, L.W. Lin, *Micropor. Mesopor. Mat.* **75**, 173 (2004)
- F. Bensebaa, N. Patrito, Y. Le Page, P. L'Ecuyer, D. Wang, *J. Mater. Chem.* **14**, 3378 (2004)
- M. Hasanpoor, M. Aliofkhaezrai, H. Delavari, *Procedia Materials Science* **11**, 320 (2015)
- L.Q. Mai, F. Yang, Y.L. Zhao, X. Xu, L. Xu, Y.Z. Luo, *Nat. Commun.* **2**, 381 (2011)
- D. Ghosh, S. Giri, M. Moniruzzaman, T. Basu, M. Mandal, C.K. Das, *Dalton Trans.* **43**, 11067 (2014)
- C. Sekar, R. Kalai Selvan, S.T. Senthilkumar, B. Senthilkumar, C. Sanjeeviraja, *Powder Technol.* **215-216**, 98 (2012)
- J. Yesuraj, A.S. Samuel, E. Elaiyappillai, P.M. Johnson, V. Elumalai, M. Bhagavathiachari, *J. Electroanal. Chem.* **797**, 78 (2017)
- X. Yan, L. Tian, J. Murowchick, X. Chen, *J. Mater. Chem. A* **4**, 3683 (2016)
- J. Yesuraj, S.A. Suthanthiraraj, O. Padmaraj, *Mater. Sci. Semicond. Process.* **90**, 225 (2019)
- D. Cai, B. Liu, D. Wang, Y. Liu, L. Wang, H. Li, Y. Wang, C. Wang, Q. Li, T. Wang, *Electrochim. Acta* **125**, 294 (2014)
- I. Shakir, M. Shahid, H.W. Yang, D.J. Kang, *Electrochim. Acta* **56**, 376 (2010)
- T. Watcharatharapong, M. Minakshi Sundaram, S. Chakraborty, D. Li, G.M. Shafiqullah, R.D. Aughterson, R. Ahuja, *A.C.S. Appl. Mater. Interfaces* **9**, 17977 (2017)
- B. Senthilkumar, R.K. Selvan, D. Meyrick, M. Minakshi, *Int. J. Electrochem. Sci.* **10**, 185 (2015)
- S. Jayasubramaniyan, S. Balasundari, P.A. Rayjada, N. Satyanarayana, P. Muralidharan, *RSC Adv.* **8**, 22559 (2018)
- L. Ma, M. Zheng, S. Liu, Q. Li, Y. You, F. Wang, L. Mae, W. Shen, *Chem. Commun.* **52**, 13373 (2016)
- M.S. Javed, C. Zhang, L. Chen, Y. Xi, C. Hu, *J. Mater. Chem. A* **4**, 8851 (2016)
- H. Sun, X. Liu, H. Yan, P. Guo, Y. Luo, Z. Zhang, Y. Lu, T. Peng, W. Wang, *CrystEngComm* **18**, 7696 (2016)
- L. Liu, L. Su, J. Lang, B. Hu, S. Xu, X. Yan, *J. Mater. Chem. A* **5**, 5523 (2017)

Publisher's Note Springer Nature remains neutral with regard to jurisdictional claims in published maps and institutional affiliations.